

Performance evaluation of single-mode fiber optic-based surface plasmon resonance sensor on material and geometrical parameters

Imam Tazi¹, Dedi Riana¹, Mohamad Syahadi², Muthmainnah¹, Wiwis Sasmitaninghidayah¹,
Lia Aprilia², Wildan Panji Tresna²

¹Department of Physics, Faculty of Science and Technology, Universitas Islam Negeri Maulana Malik Ibrahim Malang, Malang, Indonesia

²Research Center for Photonics, Nanotechnology and Materials Research Organization, National Research and Innovation Agency (BRIN), South Tangerang, Indonesia

Article Info

Article history:

Received Mar 15, 2024

Revised Jun 14, 2024

Accepted Jun 17, 2024

Keywords:

Fiber optic-based sensors
Finite-difference time-domain
Geometrical parameters
Optimization
Plasmonic materials
Surface plasmon resonance

ABSTRACT

Surface plasmon resonance (SPR) sensors are proficient at detecting minute changes in refractive index, making them ideal for biomolecule detection. Traditional prism-based SPR sensors encounter miniaturization challenges, encouraging exploration of alternatives like fiber optic-based SPR (FO-SPR) sensors. This study comprehensively investigates the effects of material and geometrical parameters on the performance of single-mode FO-SPR sensors using Maxwell's equation solver software based on the finite-difference time-domain (FDTD) method. The findings highlight the influence of plasmonic thin film materials and thickness on SPR spectrum profiles and sensitivity. Silver (Ag) demonstrates superior performance compared to copper (Cu) and gold (Au) in transmission type, achieving a sensitivity of up to 2×10^3 nm/RIU, while the sensitivities of Cu and Au are lower. Probe length and core diameter impact spectrum profiles, specifically resonance depth, without affecting sensitivity. Furthermore, variations in core refractive index influence both spectrum profiles and sensitivity. Probe types significantly affect both spectrum profiles and sensitivity, with the reflection type surpassing the transmission type. These results provide suggestions for optimizing FO-SPR sensors in biotechnological applications.

This is an open access article under the [CC BY-SA](https://creativecommons.org/licenses/by-sa/4.0/) license.



Corresponding Author:

Imam Tazi

Department of Physics, Faculty of Science and Technology, Universitas Islam Negeri Maulana Malik Ibrahim Malang

Gajayana 50, Malang, East Java 65144, Indonesia

Email: tazi@fis.uin-malang.ac.id

1. INTRODUCTION

Advancements in biotechnology, especially driven by plasmonic studies and nanofabrication technology, have led to the development of surface plasmon resonance (SPR) sensors. These sensors are capable of detecting small refractive index changes in the environment at the nanometer scale, making them well-suited for biomolecule detection [1]. Numerous commercial SPR sensor products utilize prism-based configurations that present a challenge in the context of miniaturization. Alternatively, utilizing fiber optics as surface plasmon polariton waveguides presents a promising route for miniaturizing SPR sensor development, potentially overcoming the challenges associated with prism-based configurations and offering distinct advantages in terms of miniaturization [2]. Despite this distinction, fiber optic-based surface plasmon resonance FO-SPR sensors exhibit performance comparable to prism-based SPR sensors, demonstrating high

sensitivity [3], label-free operation [4], and real-time monitoring capabilities [5]. Additionally, ongoing development progress indicates that fiber optic-based SPR (FO-SPR) sensors have enabled the examination of biomolecular interactions [6]. However, the primary challenge in establishing FO-SPR sensors resides in their design difficulties. These include determining optimal plasmonic film materials and thickness, as well as selecting parameters for the fiber optic, such as core refractive index, which could influence the numerical aperture (N.A.) and subsequently alter sensing performance. Noble metals generally exhibit excellent plasmonic properties due to the abundance of free electrons, resulting in a negative real permittivity ($Re[\epsilon_m]$) that enables the generation of plasmon waves. Moreover, it is well-known that good plasmonic materials satisfy $Re[\epsilon_m] < 0$ and $Im[\epsilon_m] \ll -Re[\epsilon_m]$, where $Im[\epsilon_m]$ represents the imaginary permittivity [7]. Besides material considerations, the geometrical parameters of probe types must be carefully considered. Several works develop modified-geometry probes such as U-shape [8], tip [9], and tapered-based designs; the resulting sensitivity of tapered probes can vary depending on the specific taper profile [10].

Therefore, modeling and simulation are necessary for designing and optimizing FO-SPR sensors before reaching the experimentation stage. This approach facilitates the reduction of trial and error and minimizes costs in experimentation. Various numerical methods can be employed to investigate plasmonic phenomena in such systems by solving Maxwell's equations in the optical media. These methods include the finite-difference time-domain (FDTD) method, finite element method (FEM), boundary element method (BEM), and discrete dipole approach (DDA) [11]. The FDTD method can calculate both near and far fields and is well known for its successful simulation and prediction of plasmonic properties. It allows for the monitoring of surface plasmon waves, whether localized or propagated, with stability, precision, and accuracy [12], [13]. Additionally, it enables the calculation of far field transmission within the FO-SPR sensors [14], [15].

The experimental setup of the FO-SPR sensor is shown in Figure 1, with transmission type in Figure 1(a) and reflection type in Figure 1(b). The simulation setup for this study is shown in Figure 2, with transmission type in Figure 2(a) and reflection type in Figure 2(b). This study aims to comprehensively investigate the main parameters affecting the performance of FO-SPR sensors using the FDTD approach. The effects of various materials and geometrical parameters are examined to understand their influence on sensor performance. First, we determine the optimal plasmonic thin film materials and their thickness. Subsequently, we analyze the sensing probe length, core diameter, and core refractive index. Additionally, different types of sensing probes, such as transmission and reflection types, are evaluated.

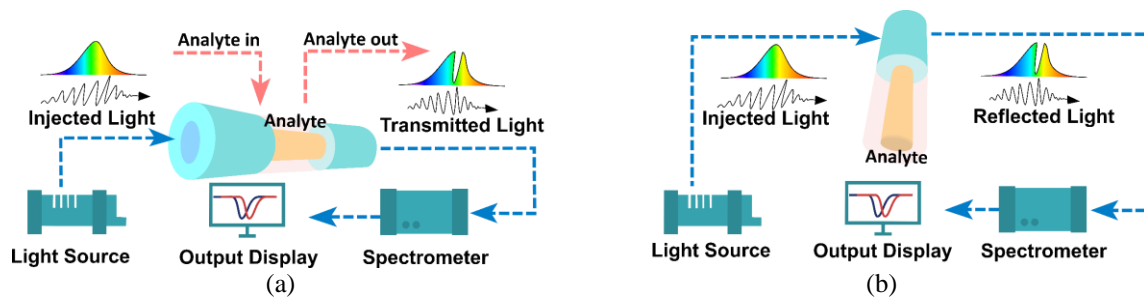


Figure 1. Schematic experimental set-up illustrating (a) transmission-type and (b) reflection-type FO-SPR sensors

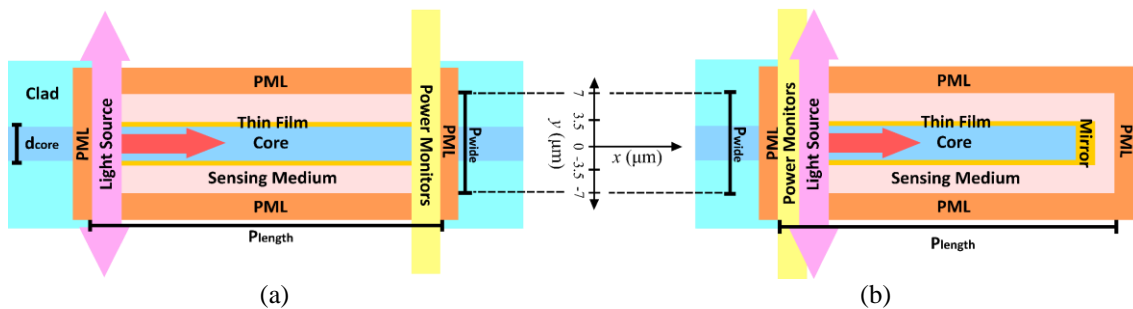


Figure 2. 2D-FDTD simulation schematics of (a) transmission type and (b) reflection type FO-SPR sensors

2. METHOD

This study used FDTD-based Maxwell's equation solver software. FDTD algorithm, also known as the Yee's algorithm, solves Maxwell's equations across space and time based on central difference approximations, enabling the calculation and storage of electric and magnetic fields within a spatial grid over time. This study comprises four stages aimed at investigating and discussing the effects of various physical parameters, including the materials and thickness of plasmonic films, probe length (P_{length}), core refractive index (RI_{core}), core diameter (d_{core}), and probe types. The first stage involves evaluating the performance of Au, Ag, and Cu plasmonic thin films and optimizing their thickness, considering variations of 20, 40, 60, and 100 nm. The second stage focuses on observing the effects of probe length variations, with lengths of 100, 200, and 300 μm . In the third stage, the study examines the impact of core refractive index (values of 1.46 and 1.52) and diameter variations (6, 8, and 10 μm). Finally, the fourth stage compares the effect of probe types, including reflection type and transmission type.

In this 2D-FDTD simulation, the structure of the FO-SPR sensor was constructed by arranging its geometrical and material components, including the core, thin film, and sensing medium (the fiber cladding is excluded as SPR phenomena occur solely within the probe area), as shown in Figure 2. The permittivity of the thin film material was fitted, using reference experimental data sourced from Johnson and Christy for Au [16], Lynch and Hunter for Ag [17], and Hagemann *et al.* [18] for Cu. The simulation area was defined with a fixed probe wide (P_{wide}) of 14 μm and the value of P_{length} according to the simulation stage. The single-mode source, with a range of broadband wavelengths from 400 to 1,200 nm, was calculated across a line and generated by a mode solver that uses the same discretization mesh as the FDTD algorithm. The selected mode typically exhibits the surface plasmon mode. Perfectly matched layer (PML) boundary conditions were applied to the simulated space, utilizing 8 layers. The mesh type was auto-nonuniform, with a minimum mesh step of 5 nm and fixed smaller mesh along the thin film (mesh override). Subsequently, the resulting transmission or reflection spectrum was recorded using a power monitor; the electric and magnetic components were used to calculate the Poynting vector, and the transmitted or reflected light power could be calculated.

3. RESULTS AND DISCUSSION

3.1. The effect of plasmonic thin film materials and thickness

The fitting permittivity models derived from experimental data for Au, Ag, and Cu can elucidate their behavior in generating surface plasmon waves, as shown in Figure 3 [7]. The real and imaginary permittivities are presented in Figure 3(a) and Figure 3(b), respectively. These plasmon waves are subject to influence from interband transitions, characterized by high imaginary permittivity across specific wavelength ranges [19]. Interband transitions, which denote the energy required for electrons to move between bands, play a crucial role in this context. Notably, Ag exhibits a comparatively smaller imaginary permittivity in the visible regime due to its higher interband transition energy of 4 eV, whereas Au and Cu possess lower interband transition energies of 2.4 eV and 2.15 eV, respectively [20]. These transitions not only impact the imaginary permittivity but also affect the energy conversion between incident light and surface plasmons [21].

In this stage, the parameters for simulated probe sensing were specified as follows: the probe type is transmission type as depicted in Figure 2(a), with a probe length (P_{length}) of 100 μm , a core diameter (d_{core}) of 6 μm , and a core refractive index (RI_{core}) of 1.46. The material and thickness of the thin film were varied to observe their effects. The power monitor at the waveguide's end, illustrated in Figure 2(a), records both the field distribution and transmission spectrum. The characteristics of the generated spectra and plasmon field by the simulated FO-SPR sensor are depicted in Figure 4. Typical SPR spectra of the generated sensor with a sensing medium refractive index (RI_{SM}) of 1.335 are shown in Figures 4(a), 4(b), and 4(c) for Au, Ag, and Cu, respectively. These spectra display varying profiles based on the material and thickness of the thin film. Two key parameters are highlighted: the transmitted power at resonance (T_{SPR}) and the full-width half-maximum (FWHM) of the resonance spectrum, as shown in Figures 4(d) and 4(e). Furthermore, Figures 4(f), 4(g), and 4(h) depict the highest magnitude of the electric field at the metal-sensing medium interface, occurring at the resonance wavelength (λ_{SPR}). This observation highlights the influence of thin film thickness on the surface plasmon mode profile, which is consistent with the transmitted power spectrum. As the thickness of the thin film increases, the resonance dip becomes shallower (or T_{SPR} increases), indicating more efficient coupling of the surface plasmon wave at specific thin film thicknesses [22]. Additionally, thicker films lead to longer resonance wavelengths. These simulation results align with previous works referenced in [23]–[26], demonstrating that increasing thickness reduces the efficiency of plasmon wave coupling at the metal-sensing medium interface. In plasmonic-based waveguides, the core mode penetrates through the metal film, facilitating surface plasmon wave coupling. However, excessively thick films hinder the efficient generation of surface plasmon waves.

As depicted in Figure 5, variations in RI_{SM} , plasmonic film materials, and their thickness result in distinct λ_{SPR} values, specifically presented in Figures 5(a), 5(b), and 5(c) for Au, Ag, and Cu, respectively. Moreover, Ag exhibits a shorter λ_{SPR} compared to both Au and Cu, while Cu shows a shorter λ_{SPR} than Au. This pattern is consistent across different film thicknesses. This phenomenon is similar to the behavior observed in localized surface plasmon resonance (LSPR), where the absorption peaks for Au as the plasmonic material appear at longer wavelengths compared to Cu and Ag [27]. Furthermore, Figure 5(d) demonstrates the sensitivity to thickness variations, with Ag providing higher sensitivity than Au and Cu. This higher sensitivity of Ag is illustrated by the steeper slope in the dispersion relation compared to Au and Cu [28]; a steeper slope in the dispersion relation typically indicates higher sensitivity because small changes in the refractive index of the medium near the metal surface result in larger changes in the momentum and energy of the surface plasmons, which are then more easily detectable. However, it is important to note that the sensitivity of the SPR sensor is not solely characterized by the dispersion relation, but rather encompasses various factors.

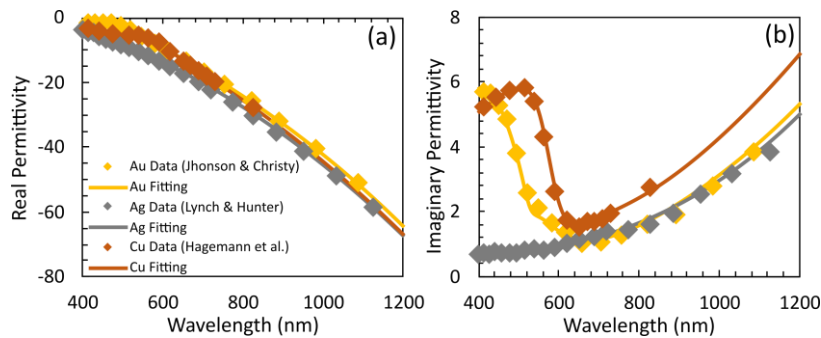


Figure 3. Experimental data and fitting models illustrating the (a) real part and (b) imaginary part of the complex permittivities for Au, Ag, and Cu

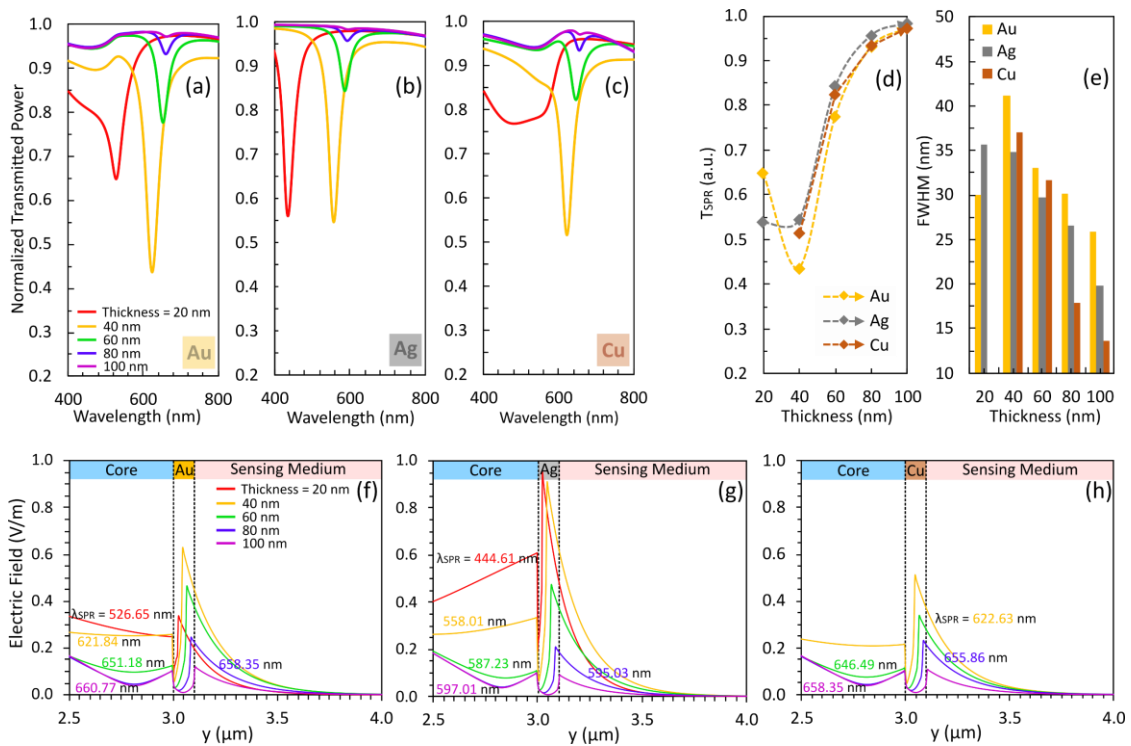


Figure 4. Transmitted power spectra of the simulated FO-SPR with (a) Au, (b) Ag, and (c) Cu thin films in various thickness. Spectrum characteristics including (d) T_{SPR} and (e) FWHM. Meanwhile, (f), (g), and (h) are visualization of electric field distributions at λ_{SPR} . Where sensing medium RI_{SM} is at 1.335

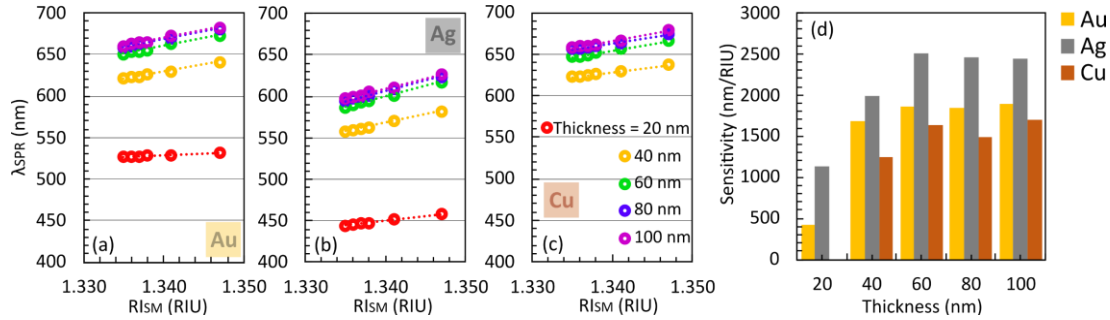


Figure 5. Resonance wavelength plotted against RI_{SM} for varying thicknesses of (a) Au, (b) Ag, and (c) Cu thin films, along with (d) their corresponding sensitivities

3.2. The effect of probe length

The length of the sensing probe is crucial because it is where the plasmonic phenomena occur and where the sensing analyte is located. In FO-SPR sensors, the cladding of the fiber optic must be removed, leaving only the core, which is then coated with the plasmonic thin film. Various tools and techniques for designing the sensing probe have been introduced in previous works. These include using a sharp blade and abrasive papers [29], a grinder with speed rotation control [30], and a controlled moving holder and flame [31].

In this stage, the effect of P_{length} on performance is discussed in a transmission type configuration, where d_{core} is set at 6 μm , RI_{core} at 1.46, and an Ag thin film thickness of 60 nm. As depicted in Figure 6, P_{length} affects spectrum characteristics. Figures 6(a) and 6(b) show that a longer P_{length} yields a deeper resonance dip. This result is consistent with previous studies using different simulation methods [23], [26], [32], and also aligns with various experimental results [29], [33], [34]. Additionally, it does not significantly change the FWHM, as shown in Figure 6(c). It highlights the crucial role of probe length in achieving a deep resonance dip. Furthermore, the electric field of the core and surface plasmon modes at λ_{SPR} on each transmission monitor (100, 200, and 300 μm) weakens as P_{length} increases, as shown in Figure 6(d). P_{length} impacts the number of reflections for light rays launched at an angle θ . Specifically, with a longer P_{length} , the number of reflections a ray undergoes also increases. With each reflection inside the SPR active region (at the core-metal interface), a certain fraction of optical power dissipates into the sensing region due to the coupling of the evanescent wave and the surface plasmon wave. This implies that with an increase in the number of reflections, there is greater decay in the power transmitted at the power monitor due to increased power dissipation [34]. However, the variation of P_{length} has no significant effect on sensitivity, as the positions of λ_{SPR} overlap for each refractive index of the sensing medium, as shown in Figures 6(e) and 6(f). Although there are slight differences in sensitivity, these are attributed to an insufficient number of wavelength interval points on the monitor, which subsequently affects the calculation of linear trends. In experimental works, concerning LSPR, it is noted that probe length does not impact sensitivity [35]. Conversely, experiments utilizing multimode fiber suggest that P_{length} affects the position of λ_{SPR} and sensitivity [36].

3.3. The effect of core diameter and core refractive index

The effects of RI_{core} and d_{core} on sensor performance are discussed in this subsection. Here, the sensing probe is in a transmission type configuration, with P_{length} set at 100 μm and the Ag thin film thickness set at 60 nm. Figure 7 and Figure 8 illustrate the effects both core diameter and core refractive index. Figures 7(a), 7(b), and 7(c) indicate that the core diameter also influences the depth of the resonance dip, with a smaller d_{core} resulting in a deeper resonance dip. This finding is consistent with the results reported by Dwivedi *et al.* [34] using multimode fibers. Additionally, the FWHM does not change significantly, as shown in Figure 7(d). A shorter core diameter leads to a stronger coupling of surface plasmon waves, as more light impinges on the thin film due to a higher number of reflections. Consequently, this results in greater decay in transmitted power. Figures 8(a) and 8(b) illustrate that the surface plasmon field at the metal-sensing medium interface is much weaker for larger core diameters, regardless of whether the RI_{core} is 1.52 or 1.46. In addition, the propagation length of the surface plasmon field with $RI_{core} = 1.46$ is longer than with $RI_{core} = 1.52$. For example, at 8 μm and $RI_{core} = 1.46$, the field still exists in the sensing medium even after passing through $y = 5 \mu\text{m}$, as shown in Figure 8(b). Meanwhile, at $RI_{core} = 1.52$, the field magnitude approaches zero around $y = 4.5 \mu\text{m}$, as shown in Figure 8(a).

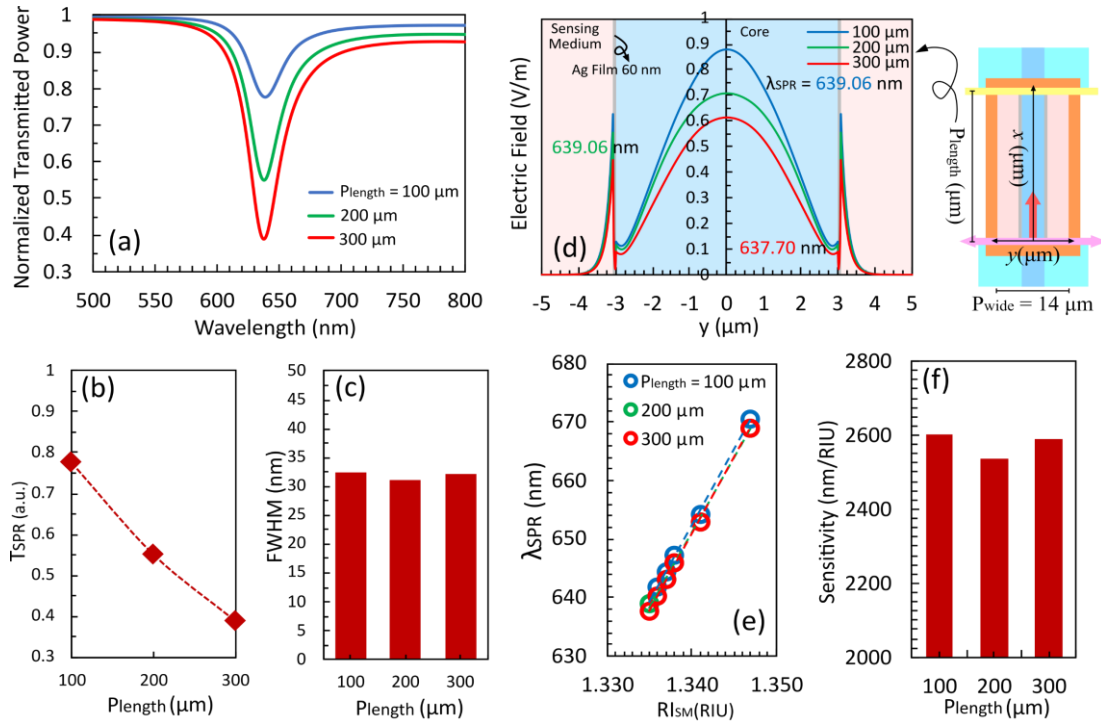


Figure 6. Simulation results investigating the effect of P_{length} on (a) transmitted power spectra, (b) T_{SPR} , (c) FWHM, and (d) electric field distributions at λ_{SPR} of the simulated FO-SPR with $RI_{SM} = 1.335$. Additionally shown are (e) λ_{SPR} versus RI_{SM} , and (f) sensitivities.

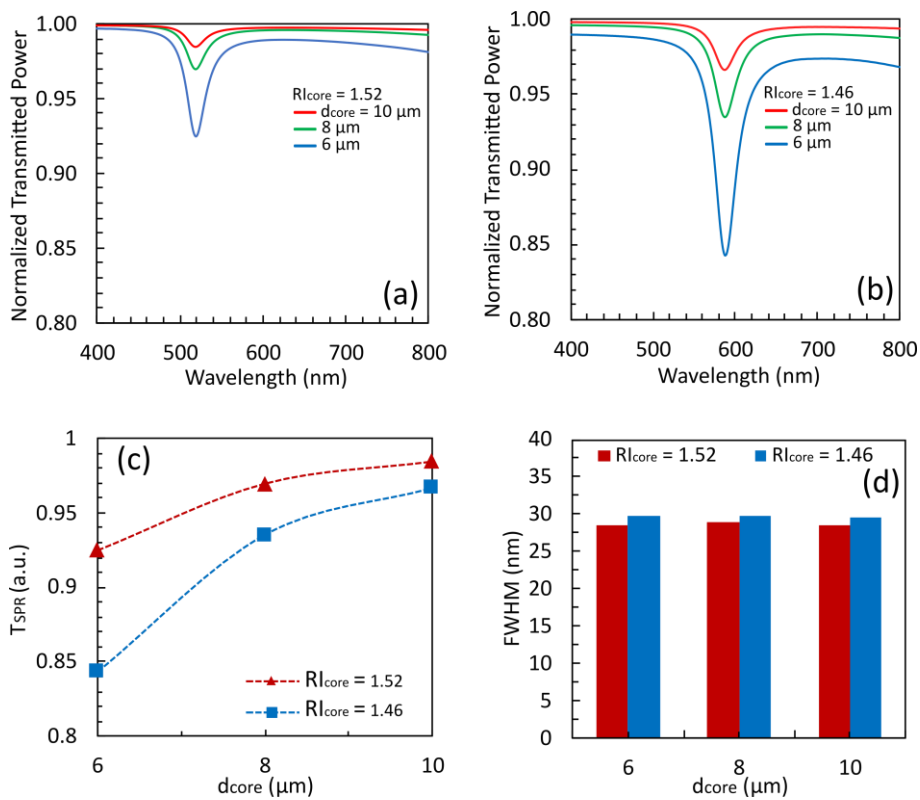


Figure 7. Transmitted power spectra with RI_{core} at (a) 1.52 and (b) 1.46, and their corresponding (c) T_{SPR} , and (d) FWHM for various P_{length} at $RI_{SM} = 1.335$

Figure 8(c) shows that variations in d_{core} do not result in a shift of λ_{SPR} within the same RI_{SM} . The λ_{SPR} values overlap, indicating that λ_{SPR} is independent of d_{core} when RI_{SM} is held constant. Meanwhile, a lower RI_{core} causes a redshift (longer λ_{SPR}). Specifically, with RI_{SM} at 1.335, the λ_{SPR} values corresponding to $RI_{core} = 1.52$ are 519.341, 519.341, and 519.247 nm for d_{core} of 6, 8, and 10 μm , respectively. However, with $RI_{core} = 1.46$, the λ_{SPR} values are 587.234, 587.635, and 587.234 nm for d_{core} of 6, 8, and 10 μm , respectively. This trend persists across all measured RI_{SM} values. These findings are consistent with experimental results reported by Liu *et al.* [37], demonstrating the direct influence of RI_{core} variations on the position of λ_{SPR} . Similarly, in prism-based SPR sensors, a lower refractive index of the prism theoretically leads to a higher resonance angle [36]. Furthermore, RI_{core} significantly affects sensitivity: it reaches over 2,000 nm/RIU for $RI_{core} = 1.46$, whereas for $RI_{core} = 1.52$, the sensitivity does not exceed 1,300 nm/RIU, as shown in Figure 8(d). This observation aligns with the findings of Liu *et al.* [37], where a lower RI_{core} is associated with higher sensitivity.

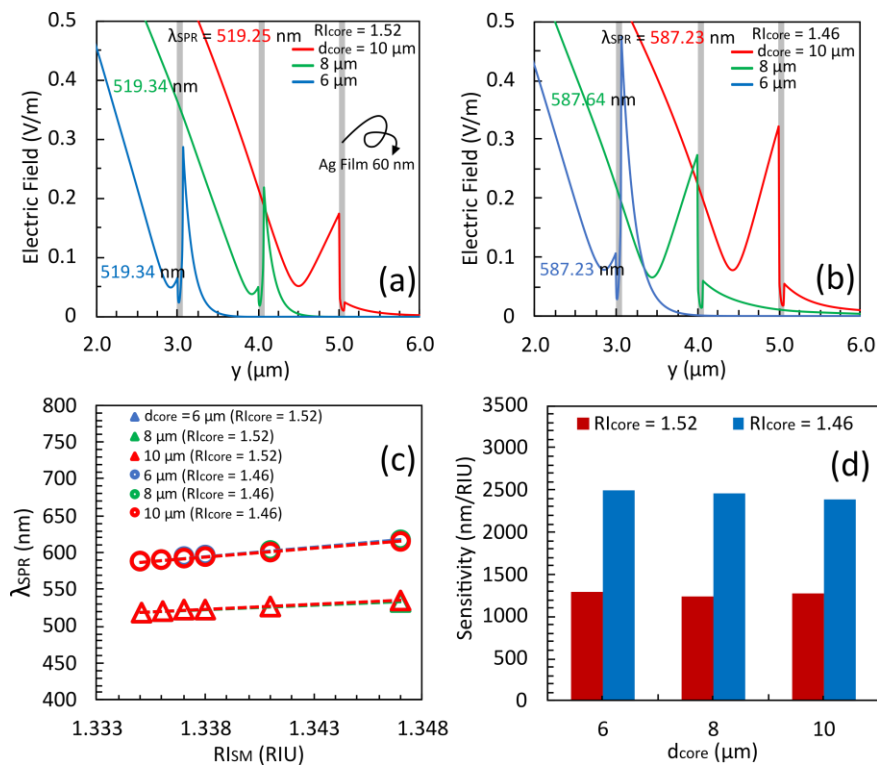


Figure 8. Electric field distribution around Ag film-sensing medium interface with RI_{core} at (a) 1.52, (b) 1.46 and $RI_{SM} = 1.335$. Additionally, the plot of (c) λ_{SPR} versus RI_{SM} , and (d) the corresponding sensitivity

3.4. The effect of probe design

Experimental investigations have demonstrated the successful application of geometry-modified probes within FO-SPR sensors. The plasmon field distribution and power in both types are presented in Figure 9. The simulation setups are shown in Figure 9(a) for the reflection type and Figure 9(b) for the transmission type, both with identical specifications: $RI_{core} = 1.46$, $d_{core} = 6 \mu\text{m}$, and $P_{length} = 100 \mu\text{m}$. In the reflection type, a 150 nm thick Ag mirror is positioned at the probe's tip, with the power monitor placed behind the injected light.

The reflection type introduces a mechanism where light traveling through the sensing probe encounters two paths, forward and backward, due to the presence of the mirror. Figures 9(c) and 9(d) illustrate the highest plasmon electric field, captured by the 2D field monitor, at around Ag film-sensing medium interface. Additionally, in the reflection type, plasmon propagation also occurs at the mirror-sensing medium interface. Figure 9(e) shows that the observed ripple pattern in the electric field magnitude signifies interference between forward and backward electric field distributions. In the transmission type, the electric field magnitude approaches half of the ripple peak seen in the reflection type, as shown in Figures 9(e) and 9(f), indicating effective light reflection by the mirror. The spectrum characteristics and sensitivity of both

designs are presented in Figure 10. The reflection spectrum exhibits a deeper resonance dip than the transmission spectrum, as shown in Figure 10(a). Correspondingly, the electric distribution of the mode within the core in transmission type at λ_{SPR} is lower in the reflection type compared to the transmission type, while the plasmon field at the metal-sensing medium interface is higher in the reflection type, as shown in Figure 10(b). Furthermore, Figure 10(c) illustrates that for the reflection type, λ_{SPR} is located at a longer wavelength than in the transmission type. Additionally, the sensitivity of the reflection type surpasses that of the transmission type, with the transmission type providing a sensitivity of 2498.90 nm/RIU, while the reflection type offers up to 2732.70 nm/RIU.

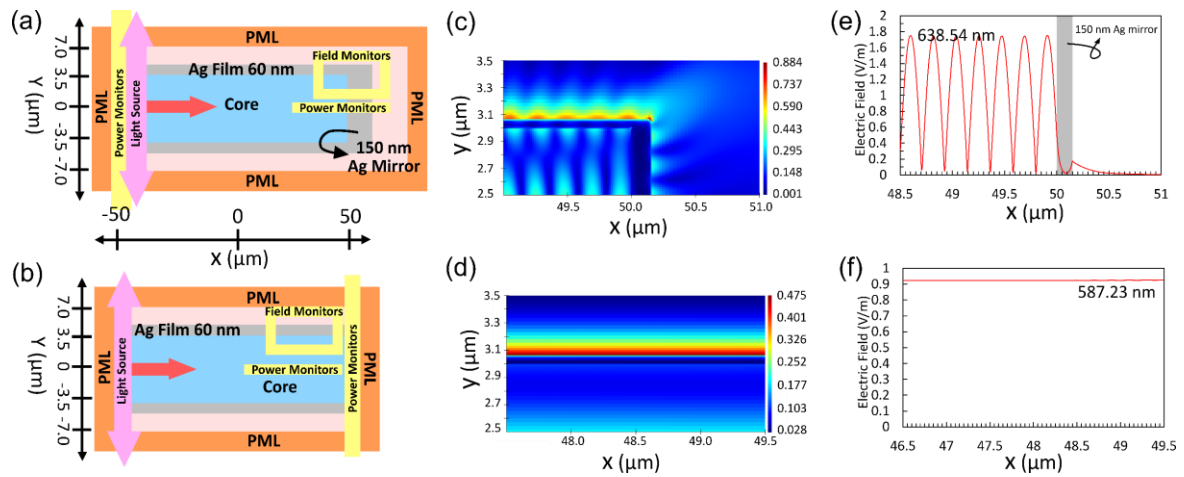


Figure 9. Simulation scheme and corresponding recorded electric field distribution by a rectangular field monitor for (a)(c) reflection type and (b)(d) transmission type, respectively. Additionally, electric field distribution at $y = 0 \mu\text{m}$ for (e) reflection and (f) transmission types are presented ($RI_{SM} = 1.335$)

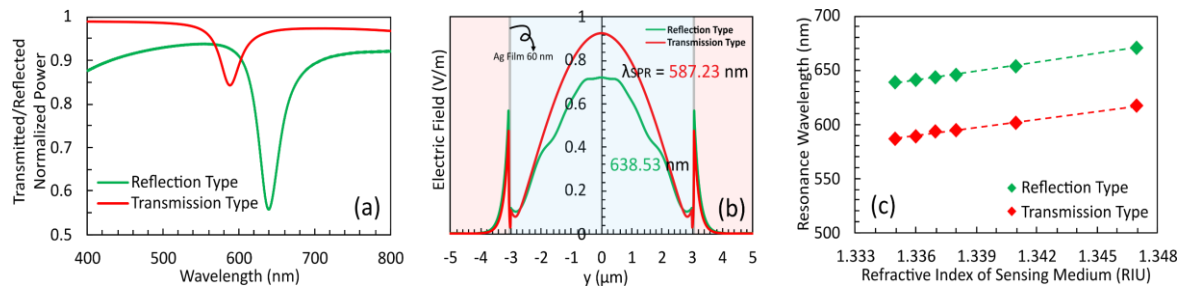


Figure 10. The recorded data from vertical power monitors, including (a) transmitted power spectra of both designs, (b) electric field distribution recorded at $RI_{SM} = 1.335$, and (c) λ_{SPR} versus RI_{SM}

4. CONCLUSION

In conclusion, this study comprehensively investigated the main parameters affecting the performance of FO-SPR sensors using the FDTD approach. Simulations examined the effects of plasmonic thin film materials, RI_{core} variations, and geometric variations (such as thin film thickness, P_{length} , d_{core} , and probe design types). Firstly, the performance of Au, Ag, and Cu plasmonic thin films with varying thicknesses was evaluated. It was found that the material and thickness of the thin film significantly influence the spectrum profile, with Ag thin film providing higher sensitivity than Cu and Au, and thicker films leading to longer λ_{SPR} . Secondly, the impact of P_{length} variations on sensor performance was investigated, showing that longer probe lengths yielded deeper resonance dips. Thirdly, the effects of d_{core} and RI_{core} on sensor performance were examined. It was observed that shorter d_{core} resulted in stronger coupling of surface plasmon waves, leading to greater decay in transmitted power, particularly in resonance dip. Additionally, variations in RI_{core} influenced the position of λ_{SPR} , with lower refractive indices associated with higher sensitivity. Finally, the study compared the performance of reflection and transmission probe types, demonstrating that the reflection type exhibited deeper resonance dips and higher sensitivity compared to the transmission type. Overall, this study

investigates key parameters influencing the performance of FO-SPR sensors, providing insights for the design and optimization for various applications in biotechnology and sensing.

REFERENCES

- [1] D. Capelli, V. Scognamiglio, and R. Montanari, "Surface plasmon resonance technology: Recent advances, applications and experimental cases," *TrAC Trends in Analytical Chemistry*, vol. 163, p. 117079, Jun. 2023, doi: 10.1016/j.trac.2023.117079.
- [2] K. Bremer and B. Roth, "Fibre optic surface plasmon resonance sensor system designed for smartphones," *Optics Express*, vol. 23, no. 13, p. 17179, Jun. 2015, doi: 10.1364/oe.23.017179.
- [3] Y. Lu *et al.*, "Beta-cyclodextrin based reflective fiber-optic SPR sensor for highly-sensitive detection of cholesterol concentration," *Optical Fiber Technology*, vol. 56, p. 102187, May 2020, doi: 10.1016/j.yofte.2020.102187.
- [4] W. Wang *et al.*, "A label-free fiber optic SPR biosensor for specific detection of C-reactive protein," *Scientific Reports*, vol. 7, no. 1, Dec. 2017, doi: 10.1038/s41598-017-17276-3.
- [5] S. Zhu *et al.*, "Real-time detection of circulating tumor cells in bloodstream using plasmonic fiber sensors," *Biosensors*, vol. 12, no. 11, p. 968, Nov. 2022, doi: 10.3390/bios12110968.
- [6] S. Kumar *et al.*, "(Invited) Advances in 2D nanomaterials-assisted plasmonics optical fiber sensors for biomolecules detection," *Results in Optics*, vol. 10, p. 100342, Feb. 2023, doi: 10.1016/j.rio.2022.100342.
- [7] P. R. West, S. Ishii, G. V Naik, N. K. Emani, V. M. Shalaev, and A. Boltasseva, "Searching for better plasmonic materials," *Laser & Photonics Reviews*, vol. 4, no. 6, pp. 795–808, Mar. 2010, doi: 10.1002/lpor.200900055.
- [8] R. Bandaru *et al.*, "U-bent fiber optic plasmonic biosensor platform for ultrasensitive analyte detection," *Sensors and Actuators B: Chemical*, vol. 321, p. 128463, Oct. 2020, doi: 10.1016/j.snb.2020.128463.
- [9] Z. Zhang, F. Chu, Z. Guo, J. Fan, G. Li, and W. Cheng, "Design and optimization of surface plasmon resonance sensor based on polymer-tipped optical fiber," *Journal of Lightwave Technology*, vol. 37, no. 11, pp. 2820–2827, Jun. 2019, doi: 10.1109/jlt.2018.2878780.
- [10] R. K. Verma, A. K. Sharma, and B. D. Gupta, "Surface plasmon resonance based tapered fiber optic sensor with different taper profiles," *Optics Communications*, vol. 281, no. 6, pp. 1486–1491, Mar. 2008, doi: 10.1016/j.optcom.2007.11.007.
- [11] M. R. Gonçalves, "Plasmonic nanoparticles: fabrication, simulation and experiments," *Journal of Physics D: Applied Physics*, vol. 47, no. 21, p. 213001, May 2014, doi: 10.1088/0022-3727/47/21/213001.
- [12] H. Y. Lee and S. N. Yi, "FDTD simulation of local electric field enhancement caused by nanoscale roughness comprising of different metals under the solar spectrum," *Journal of the Korean Physical Society*, vol. 82, no. 11, pp. 1078–1083, Mar. 2023, doi: 10.1007/s40042-023-00786-x.
- [13] F. A. A. Nugroho *et al.*, "Inverse designed plasmonic metasurface with parts per billion optical hydrogen detection," *Nature Communications*, vol. 13, no. 1, Sep. 2022, doi: 10.1038/s41467-022-33466-8.
- [14] Y. Al-Qazwini, A. S. M. Noor, P. T. Arasu, and A. R. Sadrolhosseini, "Investigation of the performance of an SPR-based optical fiber sensor using finite-difference time domain," *Current Applied Physics*, vol. 13, no. 7, pp. 1354–1358, Sep. 2013, doi: 10.1016/j.cap.2013.04.011.
- [15] C. Liu, Y. Gao, Y. Gao, Y. Wei, P. Wu, and Y. Su, "Enhanced sensitivity of fiber SPR sensor by metal nanoparticle," *Sensor Review*, vol. 40, no. 3, pp. 355–361, Apr. 2020, doi: 10.1108/sr-12-2019-0310.
- [16] P. B. Johnson and R. W. Christy, "Optical constants of the noble metals," *Physical Review B*, vol. 6, no. 12, pp. 4370–4379, Dec. 1972, doi: 10.1103/physrevb.6.4370.
- [17] D. Lynch and W. Hunter, "Comments on the optical constants of metals and an introduction to the data for several metals," in *Handbook of Optical Constants of Solids*, Elsevier, 1997, pp. 275–367, doi: 10.1016/b978-012544415-6/50015-7.
- [18] H.-J. Hagemann, W. Gudat, and C. Kunz, "Optical constants from the far infrared to the x-ray region: Mg, Al, Cu, Ag, Au, Bi, C, and Al₂O₃," *Journal of the Optical Society of America*, vol. 65, no. 6, p. 742, Jun. 1975, doi: 10.1364/josa.65.000742.
- [19] G. V Naik, V. M. Shalaev, and A. Boltasseva, "Alternative plasmonic materials: beyond gold and silver," *Advanced Materials*, vol. 25, no. 24, pp. 3264–3294, May 2013, doi: 10.1002/adma.201205076.
- [20] G. L. Eesley, "Generation of nonequilibrium electron and lattice temperatures in copper by picosecond laser pulses," *Physical Review B*, vol. 33, no. 4, pp. 2144–2151, Feb. 1986, doi: 10.1103/physrevb.33.2144.
- [21] K. Kolwas and A. Derkachova, "Impact of the interband transitions in gold and silver on the dynamics of propagating and localized surface plasmons," *Nanomaterials*, vol. 10, no. 7, p. 1411, Jul. 2020, doi: 10.3390/nano10071411.
- [22] J. Homola, "Electromagnetic theory of surface plasmons," in *Surface Plasmon Resonance Based Sensors*, Springer Berlin Heidelberg, 2006, pp. 3–44, doi: 10.1007/5346_013.
- [23] P. Mao *et al.*, "Design and optimization of surface plasmon resonance sensor based on multimode fiber," *Optical and Quantum Electronics*, vol. 47, no. 6, pp. 1495–1502, Feb. 2015, doi: 10.1007/s11082-015-0133-2.
- [24] R. Zhang, S. Pu, and X. Li, "Gold-film-thickness dependent SPR refractive index and temperature sensing with hetero-core optical fiber structure," *Sensors*, vol. 19, no. 19, p. 4345, Oct. 2019, doi: 10.3390/s19194345.
- [25] H. Suzuki, M. Sugimoto, Y. Matsui, and J. Kondoh, "Effects of gold film thickness on spectrum profile and sensitivity of a multimode-optical-fiber SPR sensor," *Sensors and Actuators B: Chemical*, vol. 132, no. 1, pp. 26–33, May 2008, doi: 10.1016/j.snb.2008.01.003.
- [26] H. Li, X. Qian, W. Zheng, Y. Lu, S. E, and Y. Zhang, "Theoretical and experimental characterization of a salinity and temperature sensor employing optical fiber surface plasmon resonance (SPR)," *Instrumentation Science & Technology*, vol. 48, no. 6, pp. 601–615, May 2020, doi: 10.1080/10739149.2020.1762204.
- [27] W. He, X. Huang, X. Ma, and J. Zhang, "Significant temperature effect on the LSPR properties of noble metal nanoparticles," *Journal of Optics*, vol. 51, no. 1, pp. 142–153, Aug. 2021, doi: 10.1007/s12596-021-00766-z.
- [28] L. C. Oliveira, C. S. Moreira, H. Neff, and A. M. N. Lima, "Optical properties and instrumental performance of thin noble metal (Cu, Au, Ag) films near the surface plasmon resonance," *Procedia Engineering*, vol. 168, pp. 834–837, 2016, doi: 10.1016/j.proeng.2016.11.285.
- [29] Y. Chen, Y. Yu, X. Li, H. Zhou, X. Hong, and Y. Geng, "Fiber-optic urine specific gravity sensor based on surface plasmon resonance," *Sensors and Actuators B: Chemical*, vol. 226, pp. 412–418, Apr. 2016, doi: 10.1016/j.snb.2015.09.056.
- [30] N. A. M. Zainuddin, M. M. Ariannejad, P. T. Arasu, S. W. Harun, and R. Zakaria, "Investigation of cladding thicknesses on silver SPR based side-polished optical fiber refractive-index sensor," *Results in Physics*, vol. 13, p. 102255, Jun. 2019, doi: 10.1016/j.rinp.2019.102255.

- [31] N. S. Aminah, S. Chalimah, Hendro, R. Hidayat, and M. Djamal, "A simulation of surface plasmon resonance-based tapered fiber and sensing," *Journal of Physics: Conference Series*, vol. 853, p. 12005, May 2017, doi: 10.1088/1742-6596/853/1/012005.
- [32] H. Lv, K. Zhang, X. Ma, W. Zhong, Y. Wang, and X. Gao, "Optimum design of the surface plasmon resonance sensor based on polymethyl methacrylate fiber," *Physics Open*, vol. 6, p. 100054, Feb. 2021, doi: 10.1016/j.physo.2020.100054.
- [33] Y. Al-Qazwini, A. S. M. Noor, M. H. Yaacob, S. W. Harun, and M. A. Mahdi, "Fabrication and characterization of a refractive index sensor based on SPR in an etched plastic optical fiber," *Procedia Engineering*, vol. 120, pp. 969–974, 2015, doi: 10.1016/j.proeng.2015.08.829.
- [34] Y. S. Dwivedi, A. K. Sharma, and B. D. Gupta, "Influence of design parameters on the performance of a surface plasmon sensor based fiber optic sensor," *Plasmonics*, vol. 3, no. 2–3, pp. 79–86, Apr. 2008, doi: 10.1007/s11468-008-9057-z.
- [35] J. Satija, N. S. Punjabi, V. V. R. Sai, and S. Mukherji, "Optimal design for U-bent fiber-optic LSPR sensor probes," *Plasmonics*, vol. 9, no. 2, pp. 251–260, Oct. 2013, doi: 10.1007/s11468-013-9618-7.
- [36] K. Brahmachari and M. Ray, "Effect of prism material on design of surface plasmon resonance sensor by admittance loci method," *Frontiers of Optoelectronics*, vol. 6, no. 2, pp. 185–193, Apr. 2013, doi: 10.1007/s12200-013-0313-2.
- [37] C. Liu *et al.*, "Fiber SPR refractive index sensor with the variable core refractive index," *Applied Optics*, vol. 59, no. 5, p. 1323, Feb. 2020, doi: 10.1364/ao.380665.

BIOGRAPHIES OF AUTHORS



Imam Tazi    received his B.Sc. degree in physics from Universitas Brawijaya, Malang, and the M.S. degree from Institut Teknologi Sepuluh Nopember (ITS), Surabaya. He also obtained Ph.D. degrees from Universitas Gadjah Mada, Yogyakarta, Indonesia. His expertise lies in sensors, particularly in the development of electronic tongues, electronic noses, and intelligent sensors for various applications such as food and environmental monitoring. Currently, he serves as the head of the bachelor's program and is an associate professor at the Department of Physics, Universitas Islam Negeri Maulana Malik Ibrahim Malang. He can be contacted at email: tazi@fis.uin-malang.ac.id.



Dedi Riana    earned a B.Sc. in physics with a concentration in electronics and instrumentation from the Department of Physics, Universitas Islam Negeri Maulana Malik Ibrahim Malang, Indonesia, in 2023. His research interests lie in optoelectronic device simulation and materials science for energy and sensing applications, particularly for solar cells, light-emitting diodes, and micro/nanosensors. Currently, he is actively involved in researching plasmonic sensors and nanophotonic simulations using Maxwell's equation solver based on finite-difference time-domain (FDTD) methods. He can be contacted via email at ddediriana@gmail.com.



Mohamad Syahadi    received his B.Eng. degree in electrical engineering from Universitas Diponegoro, Indonesia, and the M.S.Ee. degree in Electrical Engineering from the Korea Advanced Institute of Science and Technology (KAIST), Daejeon, South Korea. Currently, he is a researcher and member of the Micro Opto-Electrical-Mechanical System (MOEMS) research group at the National Research and Innovation Agency (BRIN) in Indonesia. He is interested in fiber optic sensor research based on surface plasmon resonance (SPR), integrated photonics, and electrical metrology. He can be contacted at email: mohamad.syahadi@brin.go.id.



Muthmainnah    earned her B.Sc. degree in physics from Universitas Islam Negeri Maulana Malik Ibrahim Malang, Indonesia, and the M.S. degree in physics from Institut Teknologi Sepuluh Nopember (ITS), Surabaya, Indonesia. Currently, she is an assistant professor at the Department of Physics, Universitas Islam Negeri Maulana Malik Ibrahim Malang, Indonesia, and her research interest lies in quartz crystal microbalance (QCM) sensors. She can be contacted at email: muthmainnahmsi@gmail.com.



Wiwis Sasmitaninghidayah    received her B.Ed. degrees in Physics Education Program from Universitas Negeri Malang, Indonesia, and the M.S. degree in physics from Institut Teknologi Sepuluh Nopember (ITS), Surabaya, Indonesia. Currently, she is an assistant professor at the Department of Physics, Universitas Islam Negeri Maulana Malik Ibrahim Malang, Indonesia, and her research interest lies in laser speckle imaging. She can be contacted at email: wiwishidayah87@gmail.com.



Lia Aprilia    earned her B.Sc. degree in the Department of Chemistry, Institut Pertanian Bogor (IPB), M.Eng. degree in the Department of Electrical Engineering, Universitas Indonesia, and Ph.D. degrees from the Department of Electrical Engineering, Universitas Indonesia, and the Department of Nanovision Technology, Shizuoka University, Japan. Currently, she works as a researcher in Research Center for Photonics, National Research and Innovation Agency (BRIN), Indonesia. Her research interests include microcantilever-MEMS based sensors/biosensors, surface plasmon resonance (SPR) sensor, and the development of functional materials for sensors and energy. She can be contacted at email: lia.aprilia@brin.go.id.



Wildan Panji Tresna    earned his B.Sc. degree in physics from Universitas Diponegoro, an M.Eng. degree in electrical engineering from Universitas Indonesia, and Dr.Eng. degrees from School of Electrical Engineering and Computer Science, Kanazawa University, Japan. He is a researcher and member of the MOEMS (Micro Opto-Electrical-Mechanical System) research group at the National Research and Innovation Agency (BRIN) in Indonesia. Currently, he is involved in research on optical waveguides, specifically focusing on optical encryption systems and surface plasmon resonance (SPR). This research has potential applications in halal-haram testing of products, as well as addressing environmental issues by measuring the types and levels of heavy metals in various wastewater sources. He can be contacted at email: wild004@brin.go.id.